

# ChemComm

Accepted Manuscript



This is an *Accepted Manuscript*, which has been through the Royal Society of Chemistry peer review process and has been accepted for publication.

*Accepted Manuscripts* are published online shortly after acceptance, before technical editing, formatting and proof reading. Using this free service, authors can make their results available to the community, in citable form, before we publish the edited article. We will replace this *Accepted Manuscript* with the edited and formatted *Advance Article* as soon as it is available.

You can find more information about *Accepted Manuscripts* in the [Information for Authors](#).

Please note that technical editing may introduce minor changes to the text and/or graphics, which may alter content. The journal's standard [Terms & Conditions](#) and the [Ethical guidelines](#) still apply. In no event shall the Royal Society of Chemistry be held responsible for any errors or omissions in this *Accepted Manuscript* or any consequences arising from the use of any information it contains.

## Copper-palladium core-shell as anode in a multi-fuel membraneless nanofluidic fuel cell: toward a new era of small energy conversion devices

Cite this: DOI: 10.1039/x0xx00000x

Received 00th January 2012,  
Accepted 00th January 2012

DOI: 10.1039/x0xx00000x

www.rsc.org/

J. Maya-Cornejo,<sup>a</sup> E. Ortiz-Ortega,<sup>b</sup> L. Álvarez-Contreras,<sup>c</sup> N. Arjona,<sup>a\*\*</sup> M. Guerra-Balcázar,<sup>b</sup> J. Ledesma-García,<sup>b</sup> and L.G. Arriaga<sup>a\*</sup>

**A membraneless nanofluidic fuel cell with flow-through electrodes that works with several fuels (individually or mixed): methanol, ethanol, glycerol and ethylene-glycol in alkaline media is presented. For this application, an efficient Cu@Pd electrocatalyst was synthesized and tested, resulting outstanding performance until now reported, opening the possibility of power nano-devices for multi-uses purposes, regardless fuel re-charge employed.**

Membraneless micro/nanofluidic fuel cells (MMFCs/MNFCs) also called co-laminar micro/nanofluidic fuel cells are interesting devices which exhibit advantages over traditional fuel cells related to the exclusion of ionic exchange membranes. The main challenge in MMFCs/MNFCs is to increase the cell performance. To date, the most promising pathway is using cell designs where fuel and oxidant flow through micro/nanoporous electrodes.<sup>1</sup> Several small organic molecules can be used as fuel which exhibit different theoretical energy densities such as ethanol (8030 Whkg<sup>-1</sup>), ethylene glycol (5300 Whkg<sup>-1</sup>), glycerol (5000 Whkg<sup>-1</sup>) and methanol (6100 Whkg<sup>-1</sup>).<sup>2</sup> The ideal MMFC is that which can supply the energy requirements of small devices (i.e. cellphones, cameras, etc.) as well as batteries, using the smallest possible space to allow the miniaturization of electronic devices and, at the same time, it can be operated using different organic molecules as fuel, as function of their availability. For this purpose, a versatile anode catalyst is needed. Metal mixtures between a noble and a non-noble metal are interesting because metal-metal interactions change the electronic structure of metals (with electron rearrangement occurring in the central *d*-band and in the Fermi levels)<sup>3, 4</sup> at the same time the catalyst cost is reduced. Copper, in particular is cheap and has exhibited high activity in Pd-Cu electrocatalysts.<sup>5-7</sup> Furthermore, this mixture forms weak metal-CO bonds, which is important for the regeneration of active sites on the catalyst during the oxidation of small molecules.

In this work, a Cu-Pd core-shell was synthesized, characterized and tested toward electro-oxidation of methanol, ethanol, glycerol and ethylene glycol individually and mixed in alkaline media and compared with commercial Pd/C (E-TEK). On the other hand, a

nanofluidic fuel cell was design, constructed and evaluated using Cu@Pd as anode electrocatalyst for the oxidation of these fuels at room temperature.

The Cu@Pd synthesis procedure was based on a previously reported method for the synthesis of Pd nanocubes<sup>8</sup> and is detailed in supplementary information. In brief, polyvinylpyrrolidone (PVP), sodium bromide (NaBr) and ascorbic acid (AA) were used as surfactant, additive and reductive agent, respectively. Copper sulfate and potassium tetra-chloropalladate were used as precursors. TEM images revealed that Cu@Pd/C electrocatalyst is composed of two different particle morphologies: I) core-shell semi-spherical nanoparticles and II) core-shell rod nanoparticles.

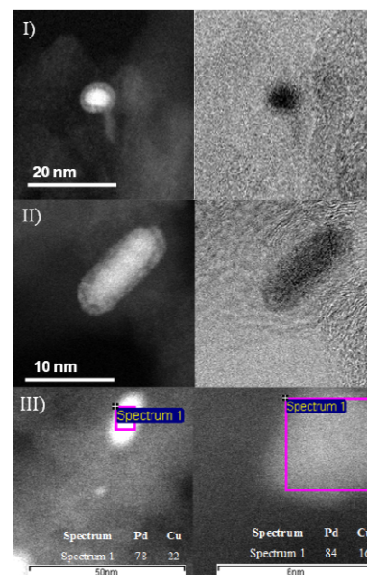


**Figure 1** HR-TEM micrographs for I) core-shell semi-spherical nanoparticles, II) core-shell nanorods and III) EDX chemical composition for Cu@Pd/C.

The average diameter of the core-shell semi-spherical particles was measured to be 6 nm, and the core-shell rods were found to be 10 nm in length. These unique morphologies were obtained due to the ability of PVP to define nanoparticle shape.<sup>8</sup> Specifically, PVP forms micelles in solution when present at certain concentrations, which enhances its ability to associate with ascorbic acid through hydrogen bonding interactions.<sup>8</sup> The ascorbic acid linked to the surface of PVP reduces the Cu ions on the surface of the micelle. After that, Pd ions engage in a redox-replacement process with the reduced Cu atoms, resulting in the core-shell morphology. The use of a bromide salt in the presence of cations such as potassium induces the formation a variety of different particle shapes, including nanobars, nanoplates and semi-spherical nanoparticles.

The elemental and mass compositions of the Cu@Pd/C electrocatalyst were determined by X-ray spectroscopy (EDX) and X-ray fluorescence (XRF) experiments, respectively. EDX analysis was performed on a single nanoparticle at a time, while the XRF data were obtained for a set of nanoparticles. With EDX, the Pd/Cu elemental ratio was found to be 84/16% for the semi-spherical particles and 78/22% for the nanorods. The high Pd content of the particles was expected because Pd forms the shells of the nanoparticles. By XRF the mass composition was of 60/40 % Pd/Cu which also indicated a higher mass composition of Pd than Cu in the particles; the agreement between EDX and XRF could evidence the formation of Cu@Pd electrocatalyst.

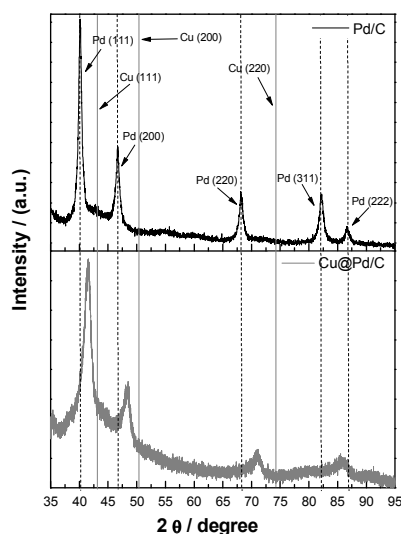


**Figure 2** X-ray diffraction pattern for Pd/C (black line) and Cu@Pd/C (grey line).

The XRD patterns for Pd/C and Cu@Pd/C are shown in Figure 2. The peaks located at  $2\theta = 41.1, 46.68, 68.24, 82.14$  and  $86.66^\circ$  are characteristics of a face-centered cubic structure for Pd and correspond to its (111), (200), (220), (311) and (222) planes (JCPDS Card #87-0638).<sup>9-11</sup> In the case of Cu@Pd/C, all of the experimentally observed characteristic peaks were shifted compared to those of the Pd/C electrocatalyst (Fig.2, black pattern). It is important to note that there are no peaks associated with Cu (JCPDS Card #04-0836)<sup>12</sup> on the XRD pattern of the Cu@Pd electrocatalyst. The average crystallite sizes were calculated using the Scherrer's equation and were determined to be 14.7 and 10.7 nm for Pd/C and Cu@Pd/C electrocatalysts, respectively. The lattice parameter of the Cu@Pd/C crystallites was calculated using the Bragg equation and was found to be 3.7483 Å. The reported lattice parameter of Pd is

3.8898 Å<sup>13</sup> and that of Cu is 3.61491 Å.<sup>12,14</sup> The Cu@Pd electrocatalyst exhibited a larger lattice parameter than metallic Cu. This behaviour could be related to the insertion of Pd into the lattice of the crystalline Cu core by a redox-replacement process related to the formation of a non-physical mixture.<sup>14</sup>

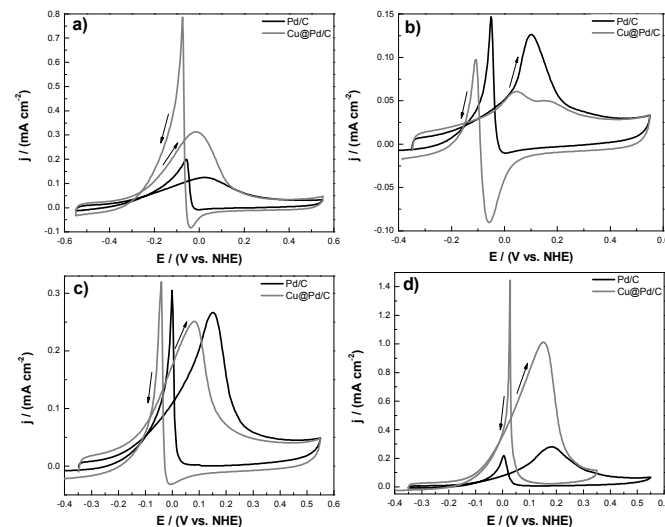
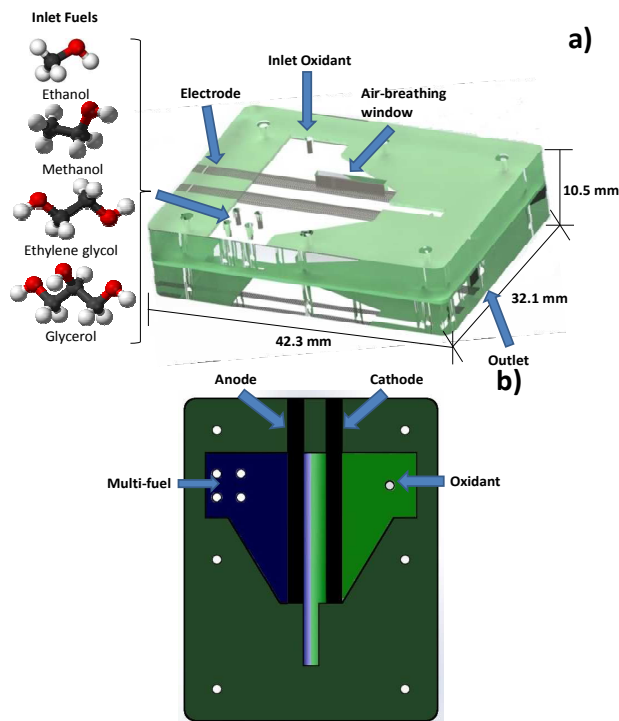


**Figure 3** Electrocatalytic activities of Cu@Pd/C and Pd/C for the electro-oxidation of a) ethanol, b) methanol, c) ethylene glycol and d) glycerol at 0.1 M.

Cu@Pd/C core-shell and Pd/C electrocatalysts were evaluated by cyclic voltammetry in acidic and alkaline media (See Fig. S1 in supplementary information). The electrocatalytic activity of the Cu@Pd electrocatalyst was tested in 0.3 M KOH (87%, J. T. Baker) using the following fuels: methanol (99.90%, J. T. Baker), ethanol (99.90%, J. T. Baker), glycerol (99.0% Sigma-Aldrich) and ethylene glycol (99.92% J. T. Baker) at four concentrations: 0.1, 0.5, 1 and 3 M for each fuel. For clarity purposes, herein only the evaluation at 0.1 M is shown in Fig. 3a to 3d, respectively. Other concentrations are shown in Fig. S2 and Table S1. Currents from electrooxidation reactions were normalized by means of electrochemically active surface area (ECSA) by integrating the charge needed to reduce a full monolayer of Pd oxides using a theoretical charge of  $405 \mu\text{C cm}^{-2}$  (see Fig. S2).<sup>15</sup> The resulting areas were of 14.049 and  $2.756 \text{ cm}^2$  for commercial Pd/C and Cu@Pd/C, respectively.

According to Fig. 3 and Fig. S2 both materials were active for the electrooxidation reactions of these fuels. In general, Cu@Pd exhibited better electrocatalytic properties than Pd/C. In the case of ethanol (Fig. 3a), the peak current density over the Cu@Pd electrocatalyst was almost 3-fold higher than over Pd/C. For methanol (Fig. 3b) conversely, the current density over Pd/C was almost 2-fold higher than that measured for Cu@Pd/C. For ethylene glycol (Fig. 3c), both materials produced similar current densities. And for glycerol as fuel (Fig. 3d), Cu@Pd/C generated a current density 4-fold higher than the output over Pd/C. The greatest improvement fostered by the Cu@Pd/C electrocatalyst was in the thermodynamic potential required for electro-oxidation to occur (Fig. 3). For the ethanol electrooxidation reaction (Fig. 3a), Cu@Pd/C and Pd/C exhibited potentials of -0.28 V and -0.18 V vs. NHE, respectively. For the methanol case (Fig. 3b), the electro-oxidation potentials were -0.07 and 0.05 V vs. NHE. In the case of ethylene glycol (Fig. 3c), Cu@Pd/C exhibited a potential of -0.1 V and Pd/C of 0 V vs. NHE. Finally, for glycerol, Cu@Pd/C showed a potential of -0.08 V and Pd/C of 0.05 V vs. NHE. In general, at 0.1

M fuel concentration, Cu@Pd/C showed a difference in onset potential greater than 100 mV compared with Pd/C. A more detailed analysis of the effect of fuel concentration was conducted and presented in the supplementary information (Table S1).



**Scheme 1.** a) Design and dimensions of the nanofluidic fuel cell and b) inlets, outlet and anode/cathode configuration.

The design of the membraneless nanofluidic fuel cell and its dimensions are shown in Scheme 1. This design is based on a previously reported.<sup>16</sup> Carbon nanofoam (Marketech International, Inc.) was used as the basis for the three-dimensional flow-through electrodes tested in this work. This material has a real surface area of  $446.4 \text{ m}^2 \text{ g}^{-1}$  as measured by BET analysis. The carbon nanofoam substrates were impregnated with the anodic and cathodic electrocatalysts by the spray technique, using 2.2 mg of Cu@Pd/C ink and 2.9 mg of Pt/C ink, respectively. The electrode dimensions were  $20 \times 3 \times 0.1 \text{ mm}$  (length, width and height). The nanofluidic fuel cell was sandwiched by two supporting plates, as shown in Scheme 1a. The top plate (I) had an air-breathing window 10 mm x 1 mm in size for taking in oxygen from the air and five additional inlets for the oxidant solution and the four fuel solutions (Scheme 1b). The bottom plate (II) had one outlet for the reaction by-products. The cell performance was normalized by the cross-sectional surface area ( $0.02 \text{ cm}^2$ ). The full description of fabrication and operation of this multi-fuel membraneless nanofluidic fuel cell is described in supplementary information (Figure S3).

The evaluation of the nanofluidic fuel cell is shown in Figure 4. All of the individual fuels and the fuel mixture were tested at a concentration of 0.1 M. This concentration was selected to study the effect of the fuel nature while avoiding possible CO poisoning effects. The polarization curves showed that all systems exhibited an open circuit potential greater than 0.6 V; the highest value of 0.670 V was achieved with the use of ethanol as a fuel.

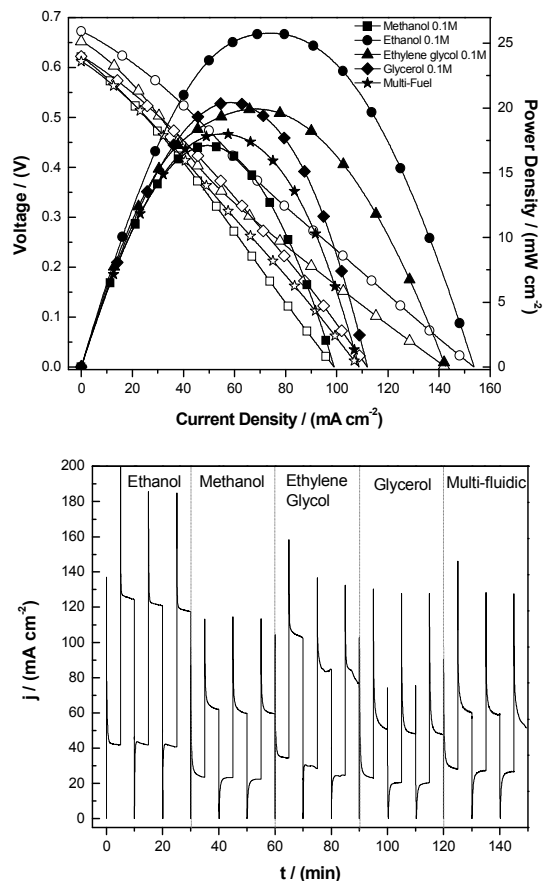


**Figure 4** Polarization and power density curves for several fuels at 0.1 M and the multi-fuel mixture used in a membraneless nanofluidic fuel cell with Cu@Pd/C as the anode at room temperature. Stability tests of device.

Additionally, the form of the polarization curves revealed that the optimal flow rates employed during nanofluidic fuel cell operation significantly reduced the occurrence of typical mass transport problems.<sup>17</sup> The highest nanofluidic fuel cell performance was also obtained for the ethanol system, while the lowest was observed using methanol as a fuel. These results could be attributed to the excellent theoretical energy density of ethanol and the comparatively low energy densities of ethylene glycol, glycerol and methanol. These less energy dense fuels introduced substantial problems to the air-breathing nanofluidic fuel cell such as cross-over effects and poisoning effects.<sup>2, 18</sup> The values of voltage, current density and power density measured are enumerated in Table S3, and it is observed that these values are higher than those reported to date. The superior power densities are the result of enhancing some important aspects of the cell, such as the use of high surface area electrodes made from carbon nanofoam, increasing the oxygen concentration by incorporating both air and dissolved oxygen into the system and enhancing the electrocatalytic properties of the anodic electrocatalyst by use of the novel Cu@Pd core-shell with semi-spherical and rod shapes.

Finally, the nanofluidic fuel cell stability was tested for a continuous flow of each fuel individually and the multi-fuel mixture (Fig. 4), operating the cell with charge and discharge potentials of 0.3 and 0.01 V, respectively. As shown in Fig. 4, it was possible to observe fuel-dependent changes in the current density. Starting with ethanol, a high current density was observed. After that, the flow of methanol

into the cell decreased the current density; the current density increased again when ethylene glycol started to flow and decreased once more due to the introduction of low-performance glycerol. Once the complete multi-fuel was flowing through the electrode, the current density increased. The multi-fuel system showed higher current density than methanol and glycerol due to the synergetic effect of fuels together. The current density remained almost constant for every fuel over duration of 150 minutes.

## Conclusions

The synthesis and integration of a highly active Cu@Pd core-shell electrocatalyst with semi-spherical and rod-shaped nanoparticles (6 and 10 nm, respectively) in a novel multi-fuel air-breathing nanofluidic fuel cell resulted in superior cell performances compared with those microfluidic fuel cells found in literature which employs ethanol, methanol, glycerol and ethylene glycol individually and mixed in alkaline media. These performances were obtained by employing the concept of flow-through electrodes using high surface area ( $450 \text{ m}^2 \text{ g}^{-1}$ ) nanoporous carbon nanofoam. In addition, the cathode performance was improved by using a combination of dissolved oxygen and air as the oxygen source. We believe that with these results, a new era in nanofluidic fuel cells can begin, where a simple device can work independently of the fuel and its availability and exhibit high performance.

## Notes and references

<sup>a</sup>Centro de Investigación y Desarrollo Tecnológico en Electroquímica, 76703 Querétaro, México.

<sup>b</sup>División de Investigación y Posgrado, Facultad de Ingeniería, Universidad Autónoma de Querétaro, 76010 Querétaro, México.

<sup>c</sup>Centro de Investigación en Materiales Avanzados S. C., 31109 Chihuahua, Mexico.

Corresponding Authors: \*[larriaga@cideteq.mx](mailto:larriaga@cideteq.mx) Tel: +52 (442) 2116069 Fax: +52 (442) 2116001; \*\*[noe.arjona@yahoo.com.mx](mailto:noe.arjona@yahoo.com.mx) Tel: +52 (442) 1921200 ext. 65421 Fax: +52 (442) 1921200 ext. 6007

† Electronic Supplementary Information (ESI) available. See DOI: 10.1039/c000000x/

1. M.-A. Goulet and E. Kjeang, *J. Power sources*, 2014, **260**, 186-196.
2. U. B. Demirci, *J. Power sources*, 2007, **169**, 239-246.
3. S. Hu, L. Scudiero and S. Ha, *Electrochem. Commun.*, 2014, **38**, 107-109.
4. T. Bligaard and J. K. Nørskov, *Electrochim. Acta*, 2007, **52**, 5512-5516.
5. W.-D. Kang, Y.-C. Wei, C.-W. Liu and K.-W. Wang, *Electrochem. Commun.*, 2011, **13**, 162-165.
6. H. Wang, R. Wang, H. Li, Q. Wang, J. Kang and Z. Lei, *Int. J. Hydrogen Energy*, 2011, **36**, 839-848.
7. C. Xu, A. Liu, H. Qiu and Y. Liu, *Electrochem. Commun.*, 2011, **13**, 766-769.
8. N. Arjona, M. Guerra-Balcázar, L. Ortiz-Frade, G. Osorio-Monreal, L. Álvarez-Contreras, J. Ledesma-García and L. G. Arriaga, *J. Mater. Chem. A*, 2013, **1**, 15524-15529.
9. T. Teranishi and M. Miyake, *Chem. Mater.*, 1998, **10**, 594-600.
10. Y. Suo and I.-M. Hsing, *Electrochim. Acta*, 2009, **55**, 210-217.
11. Y.-I. Lee and Y.-H. Choa, *J. Mater. Chem.*, 2012, **22**, 12517-12522.

12. R. Lamber, S. Wetjen and N. I. Jaeger, *Phys. Rev. B*, 1995, **51**, 10968-10971.
13. M. E. Straumanis and L. S. Yu, *Acta Cryst.*, 1969, **A25**, 676-682.
14. V. Radmilovic, H. A. Gasteiger and P. N. Ross, *J. Catal.*, 1995, **154**, 98-106.
15. T. Chierchie and C. Mayer, *J. Electroanal. Chem.*, 1982, **135**, 211-220.
16. E. Ortiz-Ortega, M.-A. Goulet, J. W. Lee, M. Guerra-Balcázar, N. Arjona, E. Kjeang, J. Ledesma-García and L. G. Arriaga, *Lab Chip*, 2014, **14**, 4596.
17. R. S. Jayashree, L. Gancs, E. R. Choban, A. Primak, D. Natarajan, L. J. Markoski and P. J. A. Kenis, *J. Am. Chem. Soc.*, 2005, **127**, 16758-16759.
18. C. J. Dyer, *J. Power Sources*, 2002, **106**, 31-34.